Soft Matter

PAPER

View Article Online
View Journal | View Issue

Cite this: *Soft Matter*, 2025, **21**, 3101

Development and characterization of a Dextran/$CaCl_2$-based blood-mimicking fluid: a comparative study of rheological and mechanical properties in artificial erythrocyte suspensions†

Gesine Hentschel, *[ab] Katharina Doll-Nikutta,[bc] Marc Mueller,[a] Philipp Berg[de] and Birgit Glasmacher[ab]

The development of accurate blood-mimicking fluids (BMFs) is essential for *in vitro* studies of blood contacting medical devices. Experimental data typically relies on single-phase glycerin/water solutions as substitutes to visualize simplified blood flow. These models are accurate only at high shear rates, limiting their applicability at lower shear rates. In this study, we investigated three potential BMFs, each composed of poly(sodium acrylate-*co*-acrylamide) hydrogel microparticles (beads) as artificial erythrocytes. Microbeads were produced using microfluidic systems (MFS) and were suspended in three plasma-like solutions: 10% and 50% (v/v) glycerol/water solutions and a Dextran40/$CaCl_2$ solution. The BMFs were evaluated for their rheological and mechanical properties, including particle elasticity, sedimentation behavior, and shear flow analysis, to assess their suitability for mimicking blood. Rheometric measurements were performed at room temperature using a plate-plate configuration, measuring viscosity and shear stress for shear rates of 5–500 s^{-1}. Atomic force microscopy (AFM) measurements were conducted to assess their mechanical response. The Dextran40/$CaCl_2$-based BMF was identified as the most promising, demonstrating rheological and mechanical properties that closely align with those of human blood. This research offers a refined approach to developing blood analogs that better simulate the mechanical response and flow characteristics of blood for the validation and development of blood contacting medical devices.

Received 20th December 2024,
Accepted 25th March 2025

DOI: 10.1039/d4sm01510j

rsc.li/soft-matter-journal

1 Introduction

Blood is a highly complex fluid, and the ability to accurately reproduce it in an experimental setting has, thus far, proven to be a significant challenge. For instance, the precise replication of blood flow is of critical importance in a number of biomedical applications, including the design of blood-contacting medical devices, the study of blood-borne diseases, and microvascular function. The complex, non-Newtonian flow behavior of blood, which is largely governed by its cellular components – most notably red blood cells (RBCs) – presents an ongoing challenge in the development of reliable blood analogs or blood-mimicking fluids (BMFs). Blood flow in varying vessel diameters, spanning from major vessels such as the *aorta* (diameter: 25 mm) or the *vena cava* (diameter: 24 mm) to microcirculatory systems (diameter: 5–10 μm), is influenced upon a multitude of blood specific properties, including shear-thinning behavior, the formation of a cell-free layer (CFL), and the deformability of RBCs in the capillary system. In large arteries, where shear rates exceed 200 s^{-1}, blood behaves predominantly as a Newtonian fluid due to the disruption of Rouleaux formation and the diminished significance of cell–cell interactions at high shear rates.[1,2] However, in smaller vessels, such as venules (shear rates 50–200 s^{-1}) and capillaries (shear rates of around 100 s^{-1}), non-Newtonian effects become increasingly dominant. This is attributed to shear-dependent aggregation of RBCs at lower shear rates, leading to shear-thinning behavior, and the formation of a cell-free layer.[2] While shear rates generally increases as vessel diameters decrease for a fixed flow rate, blood flow is not uniform across all vascular

[a] *Leibniz University Hannover, An der Universität 1, 30823 Garbsen, Germany. E-mail: hentschel@imp.uni-hannover.de; Tel: +49 511 762 3822*
[b] *Lower Saxony Centre for Biomedical Engineering, Implant Research and Development (NIFE), Stadtfelddamm 34, 30625 Hannover, Germany*
[c] *Department of Prosthetic Dentistry and Biomedical Materials Science, Hannover Medical School, Carl-Neuberg-Straße 1, 30625 Hannover, Germany*
[d] *Research Campus STIMULATE, University of Magdeburg, Sandtorstraße 23, 39106 Magdeburg, Germany*
[e] *Department of Medical Engineering, University of Magdeburg, Universitätsplatz 2, 39106 Magdeburg, Germany*

† Electronic supplementary information (ESI) available. See DOI: https://doi.org/10.1039/d4sm01510j

regions, and lower shear rates in venules allow for stronger RBC aggregation, further amplifying non-Newtonian characteristics.

Additionally, it's important to note that even in larger vessels, non-Newtonian effects can become significant in areas of flow recirculation or complex geometries (*e.g.*, curved vessels, bifurcations).[2,3] The specific properties of the RBC's such as their mechanical properties are one main reason for the complex rheology of blood, making it difficult to create a computational fluid dynamic (CFD) *in silico* model that accurately replicates real hemodynamics.[4–6]

The development of BMF's for use in experimental set-ups for flow analysis has traditionally focused on replicating the rheological properties of blood. This has been achieved using Newtonian or non-Newtonian fluid mixtures, such as water–glycerol or water–xanthan gum.[7] While these single-phase fluids offer a degree of accuracy under certain conditions, particularly at high shear rates, they fail to replicate key multiphase effects such as the axial migration of RBCs and the formation of CFLs in smaller vessel diameters. Furthermore, these fluids neglect the mechanical properties of the cells themselves, which play a critical role in the behavior of individual red blood cells in confined geometries. Human RBCs exhibit extraordinary deformability due to their biconcave shape, allowing them to squeeze through capillaries much smaller than their rest diameter. This deformability is difficult to replicate in artificial systems, yet it is crucial for understanding blood flow under physiological conditions.[8] Most of this experimentental data therefore lacks in accuracy and thus can lead to simplified and less precise simulations.

Recent advances in microfluidic technologies and the development of BMF's have sought to address these limitations. The rheological fitting of non-Newtonian flow behavior at different shear rates was achieved for different BMFs, where RBC substitutes are often polymer or hydrogel spheres.[9,10] In a recent study, Froese *et al.*[10] introduced a transparent two-phase blood model based on alginate microspheres, designed to mimic RBCs' behavior over a variety of shear rates. The model exhibited comparable shear-thinning behavior to that of blood and was capable of replicating certain features of red blood cell flow, including the formation of cell-free layers. Ghost cells (GC), erythrocytes stripped of their intracellular hemoglobin, maintain some of the rheological properties of human RBCs while offering increased but still limited optical transparency, thus making them highly suitable for visualization techniques such as particle image velocimetry (PIV).[11,12] Other approaches have sought to replicate the non-spherical shape of erythrocytes with artificial substitutes. Doshi *et al.*[13] produced concave poly(lactid-*co*-glycolid) (PLGA) microparticles with mechanical properties comparable to those of human red blood cells. In another study, Chen *et al.*[8] investigated the influence of particle shape on the flow behavior in microcirculation of artificial erythrocytes made from polydimethylsiloxane (PDMS), demonstrating the importance of particle shape in mimicking physiological erythrocyte flow. However, most existing models still fall short of achieving a more comprehensive versatility. Many of these fluids excel at

Table 1 Comparison of properties of selected blood mimicking fluids developed within the last 15 years

Base fluid (artificial plasma phase)	Material artificial erythrocytes	Particle size	Particle shape	Rheological properties	Mechanical properties	Stability over time	Ref.
Not specified	Hollow polystyrene and PLGA microparticles	7 ± 2 μm	Biconcave	Confined flow measurements to investigate deformability	1.6 ± 0.6 GPa Young's modulus	At least one week	Doshi *et al.* (2009)[13]
Saline solution matched to pig plasma osmolarity	Ghost cells (hemoglobin-deprived RBCs)	Similar to RBCs (6–8 μm diameter)	Biconcave	Matches whole blood rheology (range: 5–2500 s^{-1})	Not specified	Not specified	Schöps *et al.* (2020)[11]
Sodium dodecyl sulfate (SDS) 4% aqueous solution, Dextran 40 solution	Polydimethylsiloxane (PDMS) microparticles	7 μm	Spherical	Matches whole blood rheology (range: 1–300 s^{-1}), CFL measurements	Deformation index (DI): 0.05–0.5 (measured at different shear rates)	Not specified	Carneiro *et al.* (2021)[9]
Water–glycerol mixture with calcium chloride suspension	Alginate microspheres	20 μm (average)	Spherical	Matches whole blood rheology (range: 7–2000 s^{-1}), CFL measurements	DI 0.31 ± 0.17	Not specified	Froese *et al.* (2022)[10]
Water–glycerol mixture (36 : 64 by volume) with polyvinyl alcohol (PVA)	PDMS microcapsules with liquid core	350 μm (deflated to match RBC surface volume ratio)	Initially spherical, deflated to "buckled" shapes matching RBC deformability	Confined flow measurements to investigate deformability at different Ca numbers	Youngs modulus: 1.4 MPa–42 kPa; depending on mixing ratio	Stable for at least 6 months	Chen *et al.* (2023)[8]

reproducing either the rheological behavior or the mechanical deformation of blood components, but rarely both under the same experimental conditions. A comparison of selected BMF's properties is shown in Table 1 to emphasize the wide differences.

This research gap highlights the necessity for a more versatile blood-mimicking fluid that not only replicates the non-Newtonian rheology of blood but also incorporates the mechanical properties of deformable red blood cell analogs. The capacity to integrate these two elements into a unified model is vital for more precise simulations of blood flow, particularly in intricate or pathological scenarios, such as in stenosed vessels or during the interaction of blood with medical devices like stents and heart valves. This study introduces a novel blood-mimicking fluid designed to address these limitations by achieving the non-Newtonian rheology of blood and matching the mechanical properties of deformable RBC analogs. The fluid is composed of poly(sodiumacrylate-*co*-acrylamide) hydrogel microparticles, which are produced through microfluidic systems (MFS). To ensure optimal performance, three different plasma phases were tested as the base fluid for the suspension. The plasma phase plays a critical role in the stabilization of the suspension and the overall flow behavior of the BMF. One of the key challenges in BMF development is ensuring the stability of the particles within the fluid, particularly in preventing rapid sedimentation, which can affect the flow properties observed during experiments. To address this issue, a systematic evaluation of particle size and its influence on sedimentation behavior was conducted, ensuring that the fluid remained homogeneous before conducting any shear rate experiments. This step is crucial for maintaining the integrity of the fluid during testing, especially in long-duration or high-shear applications. The shear flow behavior of the fluid was evaluated across a range of shear rates, from low (representing venous flow) to high (representing arterial flow), thus enabling a comprehensive analysis of the fluid's rheological properties. Furthermore, the mechanical behavior of the particles was examined to characterize their mechanical response under deformation. The combination of rheological and mechanical performance experiments ensures that the BMF is capable of replicating the behavior of blood in a range of conditions, from microcirculation to larger vessels. By bridging the gap between rheological accuracy and mechanical fidelity, this work represents an advancement in the development of versatile and realistic blood-mimicking fluids for biomedical applications.

2 Methods

2.1 Microparticle fabrication

Microparticles were fabricated using MFS. The MFSs were made using the microwire molding technique (Fig. 1), as previously described by Jia *et al.*[14] To achieve the required channel geometry, which entailed an increase in channel width downstream, templates with precise dimensions were created from steel sheets with a thickness of 200 μm. The microwires were then positioned in a cross-flow configuration and PDMS, (Dow Corning, USA) was poured over them. Subsequently, the PDMS was degassed and cured at 70 °C overnight. Once the curing process was complete and the MFS has reached room temperature, the microwires were removed, resulting in inlet channels with a channel height (D_H) of 200 μm and a width (D_S) of 200 μm. The channel opening was modified downstream, with a height (D_H) of 200 μm and a width (D_W) of 400 μm Fig. 1. To facilitate the connection to tubing, needles with an outer diameter of 400 μm were inserted into the channel inlets, connecting to PTFE tubing with a diameter of 500 μm. At the outlet, a needle with an outer diameter of 800 μm was attached, connecting it to outlet tubing with a diameter of 1000 μm.

The artificial erythrocytes were synthesised using the hydrogel poly(sodiumacrylate-*co*-acrylamide) (P(SA-Am)). The concentrations of the used monomers sodium acrylate (Sigma Aldrich,

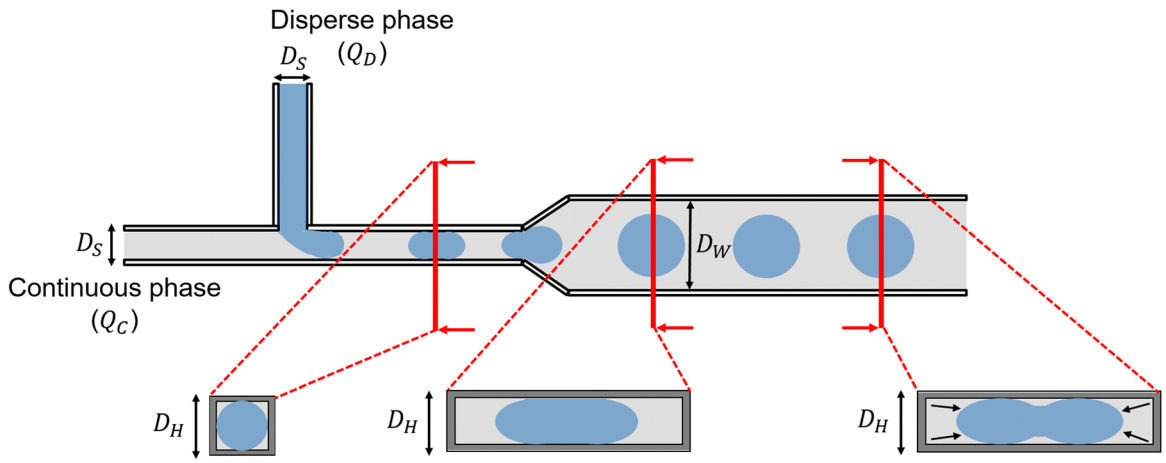

Fig. 1 Schematic representation of the microfluidic cross-section geometry. The upstream channel has a width of D_s = 200 μm and a height of D_H = 200 μm. Further downstream the channel widened into D_W = 400 μm while the height was kept at D_H. The hydrogel (blue) is introduced as the disperse phase and the mineral oil is introduced as the continuous phase (grey). The shape of the microparticles within the microfluidic system changes from a plug-like shape into a disc-like shape after the channel widens.

USA, CAS No. 7446-81-3) and acrylamide (Sigma Aldrich, USA, CAS No. 79-06-1) were 7.52% (w/v) and 17.07% (w/v), respectively. The crosslinker employed was *N*,*N*′-methylenebisacrylamide (Sigma Aldrich, USA, CAS No. 110-26-9). All components were dispersed at room temperature in distilled water and subsequently employed as the dispersed fluid phase (Q_D). The reaction starter was ammonium persulfate (Sigma Aldrich, USA, 7727-54-0), which was added directly before the start of the experiment to prevent premature gelation of the hydrogel. The continuous phase (Q_C) was mineral oil (Sigma Aldrich, USA, CAS No. 8042-47-5). *N*,*N*,*N*′,*N*′-Tetramethylethylendiamin (TEMED) (concentration 0.1% (v/v)) (Sigma Aldrich, USA, CAS No. 110-18-9) was added to the continuous phase as a catalyst for the polymerization process of the hydrogel.

To initiate particle fabrication, the disperse and continuous phases were connected to their respective inlet tubing. The flow rates were set to $Q_D = 3\ \mu L\ min^{-1}$ for the disperse phase and to $Q_C = 13\ \mu L\ min^{-1}$ for the continuous fluid phase. This configuration results in the formation of an oil–water (W/O) emulsion, which generates microparticles derived from the disperse hydrogel phase. Non-spheric shape formation was primarily controlled by the geometry of the microfluidic system and the interfacial shear forces between the two phases. This effect was maximized by the controlled flow rates, ensuring that polymerization occurred within the expansion region rather than prematurely in the narrower upstream channel or later in the outlet tubing, where shape retention would be compromised. If the particles exited the system too early, they tended to re-expand into a more spherical shape. To ensure the stabilization of the introduced shape, post-system cross-linking was achieved by adding TEMED (0.1% v/v) to the tube containing mineral oil, where the particles were collected. The catalyst promoted additional polymerization, preserving the induced non-spheric structure. The efficiency of shape retention was confirmed through microscopic analysis of multiple production batches using a USB microscope (CIMELR Digital Microscope, China), demonstrating high reproducibility. After particle production, the microparticles were washed three times. The particle shape was investigated using an inverted microscope (Zeiss, Axio Vert A1) and a scanning electron microscope (SEM) (Hitachi, S3400N, Hitachi, Japan).

2.2 Diameter distribution

The artificial erythrocytes were dispersed in the artificial plasma phase following the production of particles. The effects of three different plasma phases on the swelling of the artificial erythrocytes were investigated. Two plasma phases consisted of glycerol/water suspensions at two glycerol concentrations: 10% (v/v) and 50% (v/v). These concentrations, along with other glycerol/water solutions in the 10–60% (v/v) range, have previously been employed as single phased blood-mimicking fluids for computational fluid dynamics (CFD) simulations in several studies.[5,15,16] These solutions increase the viscosity of the suspending medium. A third plasma phase, designed to additionally replicate intercellular interactions in blood due to plasma proteins was prepared by combining 10 mM $CaCl_2$ with Dextran 40 (Sigma Aldrich, USA) in a 90%/10% (v/v) ratio, following the methodology of Fukada *et al.*[17] Unlike glycerol-based solutions, which primarily affect viscosity, this phase was specifically formulated to mimic physiological cell aggregation effects observed in blood. The Dextran 40 acts as an interparticle bridging agent, forming weak, reversible bonds between artificial erythrocytes, similar to how fibrinogen mediates RBC aggregation in human blood plasma. The $CaCl_2$ is used to influence particle–particle interactions, as well as the ionic strength of the artifical plasma phase. Artificial erythrocytes were suspended in each plasma phase and allowed to swell for 48 hours at room temperature (22 °C), in accordance with the findings of Hentschel *et al.*,[18] which demonstrated that microparticle swelling reaches a threshold after 48 hours. Additional information on the swelling behavior of the hydrogel in the different plasma phases can be found in S1 of the ESI.† A control group (n = 1700) was prepared by suspending the artificial erythrocytes in fresh mineral oil. The diameters of the particles were measured microscopically to assess their size. To ascertain the statistical significance of the observed differences, the commonly used Kolmogorov–Smirnov and Shapiro–Wilk tests were conducted to assess data log-normality. The Kruskal–Wallis test was then employed to determine if there was a significant difference in particle diameters between erythrocytes swelled in artificial plasma phases and those maintained in mineral oil.

2.3 Rheological characterization

2.3.1 Sample preparation and rheological set-up. The bead volume fraction of each BMF was set to 40% (v/v) to closely mimic physiological hematocrit levels. All measurements took place 48 h after particle fabrication to ensure complete particle swelling. The rheological characterization of the three BMFs was carried out at room temperature (22 °C). This approach follows established methodologies in BMF research, where rheological measurements are often performed at room temperature to ensure stability, experimental reproducibility, and ease of application in *in vitro* studies.[9,16] Additionally, many experimental blood flow studies are conducted at 22 °C[19–21] to simplify setups and avoid the need for additional temperature control. This approach not only simplifies future experimental use but also minimizes the risk of swelling or deswelling effects due to temperature variations. All experiments were conducted using a rotary rheometer (Kinexus Prime Ultra+, NETZSCH GmbH, Germany) with a 40 mm plate-plate geometry. The plate-plate geometry was chosen due to the particle size of the tested BMFs. While this geometry may introduce minor flow field inconsistencies, these effects are negligible compared to the measurement inaccuracies that arise from the non-negligible particle-to-gap size ratio in alternative rheometer geometries. A solvent trap was employed to prevent evaporation. To increase the homogeneity of the BMFs before the rheological measurements, they were agitated for 50 s at $100\ s^{-1}$.

2.3.2 Particle sedimentation under constant flow. The impact of sedimentation under constant shear was examined,

Table 2 Adjusted plate distances for the three blood mimicking fluids

Blood mimicking fluid	Plate distance in mm
Dextran40/$CaCl_2$	1.5
Glycerol 10% (v/v)	2.5
Glycerol 50% (v/v)	3

as sedimentation behavior can significantly impact shear flow dynamics. To assess the impact of particle sedimentation on viscosity, the dynamic viscosity of the three BMF was monitored over time. The measurements were taken at four discrete shear rates (1, 10, 100, and 200 s^{-1}) over an observation period of 10 minutes, with viscosity values recorded every 10 seconds under constant shear. In order to accommodate the varying particle sizes present across the three BMFs, the plate distance was adjusted accordingly. The specific distances employed for each BMF are provided in Table 2. The rheometer gap distance was carefully optimized prior to experimentation, to balance bulk suspension behavior while maintaining sample stability. For this, the gap distance was systematically tested to determine the maximum feasible distance were consistend measurement was still possible. The normal force measurements were tracked as an indicator to identify fluid loss between the plates. A drop in normal force was considered an indication that the liquid phase was escaping, necessitating a reduction in gap size to maintain measurement integrity. Conversely, smaller gap sizes were also tested, but they introduced measurement artifacts due to confinement effects, as additionally indicated by rheometer software warnings.

2.3.3 Dynamic shear behavior. The dynamic flow behavior of the three BMFs was investigated under constant shear at varying shear rates. Shear rates were incrementally increased from 5 to 500 s^{-1} with a step width of 5 s^{-1}, and each step was held for at least 10 seconds to allow the fluid to reach a steady state. When the steady state is reached, viscosity and shear stress are measured and the next shear rate step is approached. As a control, porcine whole blood (hematocrit: 46% (v/v)) was tested. Porcine blood is widely used as a reference in *in vitro* flow studies due to its close physiological resemblance to human blood, combined with its accessibility, ease of handling, and cost-effectiveness. These attributes make it a practical and reliable model for replicating human blood flow dynamics in laboratory settings.[22] Coagulation was inhibited by adding 5% (v/v) citrate. This addition slightly reduced the overall viscosity of the blood sample. Porcine whole blood was measured at physiological temperature (37 °C).

To characterize the flow behavior of each BMF, two established flow models to describe the shear flow of blood, the Casson and Carreau–Yasuda models, were applied to the shear flow data.[23,24] The Casson model is defined as:

$$\sqrt{\tau} = \sqrt{\tau_y} + \sqrt{\eta_\infty \dot{\gamma}} \quad (1)$$

where τ represents the shear stress (in Pa), τ_y is the yield stress (in Pa), η_∞ is the infinite shear viscosity (in Pa s), and $\dot{\gamma}$ is the shear rate (in s^{-1}). The values for τ_y and η_∞ were extracted from the fitted curves and compared to the control and compared to literature values, with the coefficient of determination (R^2) calculated to assess the quality of the fit. Additionally, the experimental data was fitted against a second model. The Carreau–Yasuda model is particularly suited for fluids exhibiting pseudoplastic behavior, such as biopolymer solutions, protein solutions, and polymer melts, where the fluid undergoes shear thinning. The Carreau–Yasuda model is expressed as:

$$\eta = \eta_\infty + (\eta_0 - \eta_\infty)[1 + (\lambda\dot{\gamma})^a]^{(n-1)/a} \quad (2)$$

where η is the viscosity (in Pa s), η_0 is the zero-shear viscosity (in Pa s), η_∞ is the infinite–shear viscosity (in Pa s), λ is the time constant (in s), $\dot{\gamma}$ is the shear rate (in s^{-1}), a is the transition control factor, and n is the power index. The initial values used for fitting human whole blood were based on literature values:[25] η_0 = 0.02 Pa s, η_∞ = 0.003 Pa s, λ = 1 s, a = 2.5, and n = 0.6.

2.4 Mechanical characterization

The mechanical response and elasticity of artificial erythrocytes were assessed using atomic force microscopy (AFM) (Flex FPM, Nanosurf AG, Liestal, Switzerland). Repeated indentation measurements were conducted to calculate Young's modulus, representing the elasticity of the cells, and to evaluate deformability under repeated mechanical load. Porcine erythrocytes served as a positive control for comparison.

The AFM system was equipped with hollow silicon nitride cantilevers. For the artificial erythrocytes, cantilevers with an opening of 8 μm and a theoretical spring constant of 2 Nm^{-1} were used (FluidFM Nanopipette, Cytosurge AG). For porcine erythrocytes, cantilevers with a pyramidal tip and an opening of 300 nm with a theoretical spring constant of 0.6 Nm^{-1} were applied. Artificial erythrocytes and porcine erythrocytes were dispersed to 1% in their artificial plasma phase and phosphate buffered saline solution (PBS), respectively. Measurements were conducted after the artificial and porcine erythrocytes had sedimented in flat 40 mm diameter WillCo-dishes (WillCo Wells B.M., Amsterdam, Netherlands), and target particles were selected microscopically. For each BMF and the control, 15 individual cells were examined. For each cell, 10 force spectroscopy curves were recorded with a setpoint force of 50 nN for artificial erythrocytes and 1 nN for porcine erythrocytes, an approach/withdrawal velocity of 1 μm s^{-1}, and force feedback enabled.

The resulting force–distance (here: indentation of particle surface) curves were analyzed using AtomicJ 1.7.2 software. Exemplatory curves are shown in S3 of the ESI.† Quality control procedures were implemented to exclude curves showing inconsistencies, such as cantilever slippage or adhesion on the microparticle/erythrocyte surface. The force–distance curves were plotted to analyze approach and withdrawal behavior, with detailed plots available in the ESI,† S3. Young's modulus, representing cell elasticity, was derived from the approach curves. The slope of the linear elastic region of the curve was determined,[26] typically the initial straight portion.

Young's modulus was than calculated from:

$$E = \frac{F/A}{\Delta L/L} = \frac{FL}{A\Delta L} \quad (3)$$

where E is the Young's modulus (in Pa), F the applied force (in N), A the cross-sectional area (in μm^2), L the original diameter (in μm) and ΔL the change in length (here indentation) (in μm), using the slope determination from the force-way curves. Statistical analysis was performed to test for significant differences in elasticity between the artificial and porcine erythrocytes. Kolmogorov–Smirnov and Shapiro–Wilk tests were conducted to check for log-normality of the data, followed by a Kruskal–Wallis test to determine whether the Young's modulus of the artificial erythrocytes differed significantly from that of the positive control.

3 Results and discussion

3.1 Microparticle fabrication

Two particle morphologies were determined within the MFS. The first of these is a plug-like shape, as observed in the upper downstream channel with the diameter D_S (Fig. 1). The dispersed fluid phase completely occupies the volume of the upper channel. The microparticle break-up is dependent upon the interfacial pressure increase that occurs at the cross-section geometry.[27] The length of the resulting plug is greater than the length of the channel diameter D_S. The interfacial tensions between disperse and continuous phase lead to particles with plug like shape within the cross-section of the small upstream channel (Fig. 1). This is in accordance with the findings of Dendukuri *et al.*,[28] who observed that particle polymerization within this area exhibits a plug like geometry. Furthermore, at the point of widening of the downstream channel, the microparticles assume a disc-like shape (Fig. 2). In this area, the microparticles are confined in two dimensions (top and bottom), resulting in their non-spherical form. This behavior has been previously reported by Dendukuri *et al.*[28] and Winkler *et al.*[29] and can also be observed within this experimental setup.

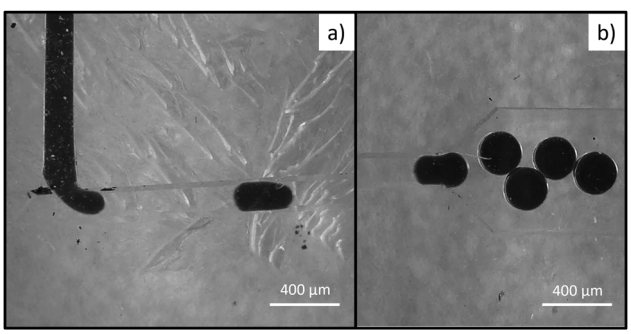

Fig. 2 Two particle morphologies were determined within the microfluidic system. (a) In the D_S channel area the particle takes on a plug-like shape governed by the interfacial tensions of disperse and continuous phase. (b) After the widening of the downstream channel the microparticle shape is disc-like, confined by the upper and lower channel walls.

The hydrogel microparticles undergo polymerization within the MFS while flowing downstream, resulting in a non-spherical morphology upon exiting the MFS. Microscopic examination reveals the presence of an indentation in the microparticles, mimicking the biconcave shape in human red blood cells (Fig. 3). To corroborate the concave morphology of the microparticles, supplementary scanning electron microscopy images were obtained. As illustrated in Fig. 3, an indentation is evident on the surface of the microparticle. Furthermore, an additional indentation is visible on the opposite side, at the base of the structure. This confirms the biconcave shape of the microparticles. However, the indentation appears less pronounced compared to the light microscopy images. This observation can be attributed to the specific environment required for the execution of SEM measurements. Before analysis, it is necessary to dry the microparticles. Given their high water content, microparticles may undergo shrinkage during the drying process. This phenomenon may be attributed to the altered shape of the microparticle. Additionally, the high-vacuum environment present in the SEM can further influence particle morphology.

The formation of the biconcave structure is attributed to the polymerization dynamics within the MFS. The polymerization process is governed by free radical polymerization, initiated in the presence of a catalyst within the continuous phase. The specific shape of the microparticles is likely a result of differential polymerization rates across the particle surface, which are influenced by diffusion limitations within the microfluidic channel. The presence of the catalyst in the continuous phase governs polymerization from the outside to the inside. As the particles flow within the microchannel, they remain confined near the top and bottom channel walls, where a thin lubricating layer of mineral oil is present. This lubrication layer serves as a diffusion barrier, reducing catalyst availability in the top and bottom regions and leading to slower polymerization at these regions to the sides, where direct contact with bigger volume of the catalyst-rich continuous phase allows for faster polymerization (Fig. 1). As the microparticles exit the microfluidic system, unpolymerized or weakly crosslinked material in the top and bottom regions is more susceptible to removal during the washing steps, resulting in the final biconcave shape.

The biconcave shape of erythrocytes plays a pivotal role in optimising blood flow in different vessel geometries. In large vessel geometries, the erythrocyte shape facilitates laminar flow by increasing the cells' moment of inertia, thereby reducing particle rotation within the flow.[30] In narrow vessels, the biconcave shape enhances their efficient passage. Additionally, the area-to-volume ratio is increased, thus enhancing the efficiency of gas exchange.[31]

3.2 Diameter distribution

To evaluate the impact of different artificial plasma phases on the size and swelling behavior, their diameter was compared to the median diameter of the artificial erythrocytes in the control condition (mineral oil). Their diameter was observed to be 294 μm. In contrast, hydrogel beads dispersed in the Dextran

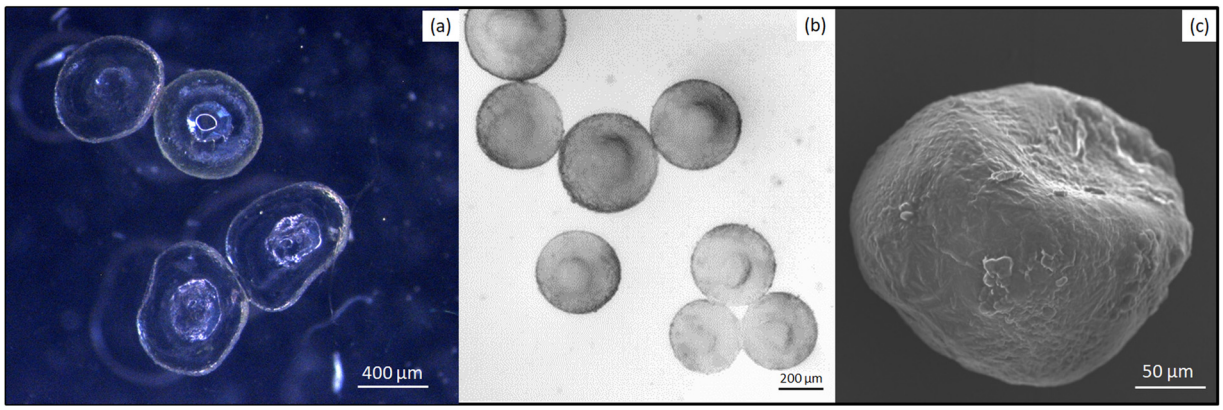

Fig. 3 (a and b) Light microscopic image of the produced microparticles. An indentation in the particle surface is visible. (c) SEM image of a microparticle showing the biconcave shape.

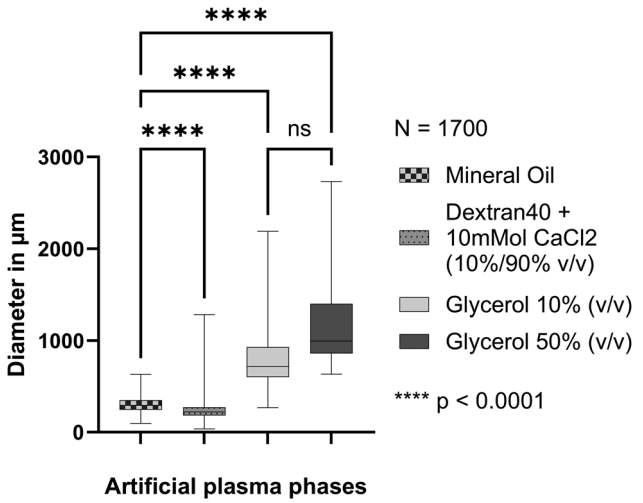

Fig. 4 Diameter distribution of artificial erythrocytes dispersed in the investigated artificial plasma phases. All particle diameters were measured after 48 h of swelling in the respective plasma phases.

40/$CaCl_2$ solution exhibited a significantly reduced diameter, with an average of 222 µm (Fig. 4). This considerable reduction in diameter can be attributed primarily to two factors: a diminished capacity for swelling and augmented ionic cross-linking. Mahon *et al.*[32] demonstrated that higher salinity reduces the swelling capacity of hydrogels, which they attributed to a decrease in osmotic pressure due to additional cations, which inhibit water uptake. This effect is likely to play a role in the interactions between P(SA-Am) and $CaCl_2$, where the hydrogel's anionic repulsion is counteracted by the cations present in $CaCl_2$, thereby reducing its potential for water absorption. Furthermore, as reported by Trivedi and Chourasia,[33] hydrogels with exposed hydrophilic groups form complexes with cations when exposed to $CaCl_2$ solutions. This results in the formation of additional ionic cross-links that increase the density of cross-links and further restrict hydrogel swelling. For P(SA-Am) beads, it can be assumed that ionic cross-links were formed between the carboxylate groups ($-COO^-$) from sodium acrylate, which would explain the observed reduction in swelling ability.

The artificial erythrocytes showed significantly enhanced fluid uptake in glycerol/water solutions, with final median diameters of 718.43 µm in the 10% (v/v) glycerol solution and 997.44 µm in the 50% (v/v) glycerol solution. This resulted in particles that were three to four times larger than those observed in dextran 40/$CaCl_2$. A study by Bialik-Was *et al.*[34] observed that higher glycerol concentrations within the hydrogel matrix can reduce particle swelling, the opposite trend was noted here when the glycerol was present in the surrounding phase, with the 50% (v/v) glycerol solution resulting in slightly larger particles than the 10% (v/v) solution. Nevertheless, the statistical analysis revealed no statistically significant difference in diameter between the two glycerol concentrations, indicating that any observed size differences are likely due to other factors rather than being attributable to glycerol concentration alone (Fig. 4).

These findings highlight the considerable impact of the surrounding plasma phase on the final diameter of artificial erythrocytes. It was observed that the particles swell immensely in the glycerol solutions, while the combined impact of $CaCl_2$'s swelling inhibition and ionic crosslinking in Dextran 40/$CaCl_2$ solutions even lead to a diameter decrease compared to the positive control. This distinction highlights the importance of ionic content and cross-linking potential in modulating hydrogel particle size and swelling behavior, with significant implications for applications requiring precise control over microparticle size.

While particle sizes across all fluids remain larger than the target size of 8 µm, the Dextran 40/$CaCl_2$ model achieved the smallest particles among the three. While the hydrogel particles are significantly larger than natural red blood cells, this does not exclude their potential utility as a BMF in flow simulations. In fact, the need to upscale vessel diameters is common in both experimental and computational hemodynamic studies. A study by Wu *et al.*[35] on intracranial aneurysms highlights the necessity of scaling up vessel

geometry to increase spatial resolution in some PIV experiments. Goubergrits *et al.*[36] demonstrates how maintaining hydrodynamic similarity through Reynolds number matching can allow for accurate flow representation despite geometric scaling. A scaling factor of 3.77 was applied to an intracranial aneurysm model for *in vitro* testing using water–glycerol mixtures, ensuring dynamic similarity and maintaining correct flow structures even with larger dimensions. Many *in vitro* models, such as those used for medical device testing, require upscaled features to ensure reproducibility and proper visualization of flow phenomena.

When investigating complex hemodynamic phenomena, larger-scale models provide advantages by mitigating resolution limitations and ensuring that the flow structures of interest remain within the detectable range of experimental techniques. In this context, upscaled particles would be beneficial and can effectively be used to mimic the multiphase properties of blood.

Reducing particle size to more closely match human erythrocytes will require further optimization, potentially by reducing channel diameters in the microfluidic fabrication process. Kašpar *et al.*[37] demonstrated that a decrease in the overall channel diameter, achieved by increasing the aspect ratio of the channel walls, results in a reduction in the size of the produced particles. A further study by Tanriverdi *et al.*[38] demonstrated that the monodispersity of the produced particles increased with decreasing channel size. The elastic forces acting on the particles increase, leading to enhanced focusing of the particles at the center of the channel and a reduction in coalescence effects.

3.3 Rheological characterization

3.3.1 Particle sedimentation under constant flow. The experiments were conducted based on the hypothesis that particle sedimentation within a solution would result in a decrease in overall viscosity. This hypothesis aligns with the findings of Momen-Heravi *et al.*[39] and Shajahan and Breugem.[40] To investigate this effect, the dynamic viscosity of the BMFs was monitored over a 10-minute period at different shear rates. Both absolute and normalized dynamic viscosity values were plotted against measurement time. To compare the effect of constant shear flow on the viscosity changes we calculated the sedimentation velocity under quiescent conditions (the caluclation protocol is described in the ESI,† S2). Which were 0.0451 mm s^{-1}, 0.232 mm s^{-1} and 0.218 mm s^{-1} respectively, for the Dextran 40/$CaCl_2$ model, the 10% (v/v) glycerol and the 50% (v/v) glycerol model. The sedimentation velocity increases with particle diameter. However, these estimates are only a rough approach due to the biconcave shape of the artifical erythrocytes. A study by Oka *et al.*[41] shows the change in effective radius reduces the sedimenation velocity according to Stokes' law.

The dynamic viscosity of the microparticles – Dextran 40/$CaCl_2$ solution displays fluctuations at low shear rates (1 s^{-1}) within the flow field (Fig. 5). Which is visible in both viscosity graphs. These fluctuations are likely due to the time required for the flow field to fully develop within the plate–plate geometry. For the Dextran 40/$CaCl_2$ BMF, transient effects were observed, characterized by a peak in viscosity approximately 1 minute after measurement initiation at 1 s^{-1}. Following this peak, viscosity decreased to a normalized value of 0.87, accompanied by fluctuations throughout the measurement period. This suggests a slight sedimentation effect, while the fluctuations indicate intermittent particle resuspension under shear flow. The sedimentation effect may be attributed to density differences between the hydrogel microparticles and the plasma phase (for density determination details, see ESI,† S2). The density of Dextran 40/$CaCl_2$ was 0.9992 g cm^{-3}, while that of the hydrogel particles was 1.0781 g cm^{-3}, corresponding to a 7.9% density difference. However, compared to the sedimentation velocities at quiescent conditions the sedimentation effects are less pronounced than expected. Sedimentation velocity seem to be slowed even at low shear velocities. While considerable scatter among viscosity measurements at a shear rate of 1 s^{-1} emphasizes flow inconsistencies, the average viscosity over the whole measurement period was at around 0.155 Pa s. This value is higher than the viscosity of human whole blood, which has been reported as 0.06 Pa s at 0.1 s^{-1} by Nader *et al.*[42] This indicates that the BMF displays enhanced resistance to flow under low-shear conditions. This resistance can potentially be attributed to interparticle bridging effects induced by the Dextran 40. At a shear rate of 10 s^{-1}, viscosity fluctuations persisted during the first three minutes, likely due to start-up effects commonly observed in plate–plate rheometry and the higher resistance to flow in the Dextran 40/$CaCl_2$ solution. The normalized viscosity data supports this interpretation; after approximately 240 seconds, fluctuations diminished, and the normalized viscosity stabilized around 1, indicating no significant sedimentation effect at this shear rate. The average viscosity at 10 s^{-1} decreased significantly compared to 1 s^{-1}, with a measured value of 0.011 Pa s, demonstrating shear-thinning behavior.

At higher shear rates (100 and 200 s^{-1}), viscosity remained stable over time, with no significant decrease in normalized viscosity, confirming the absence of sedimentation effects. The average viscosity at 100 s^{-1} was 0.0091 Pa s, which further decreased to 0.0063 Pa s at 200 s^{-1}. These values align closely with the viscosity of human blood at equivalent shear rates, as reported by Nader *et al.*[42] (0.006 Pa s at 200 s^{-1}). Additionally, the shear-thinning effect was more pronounced between 10 and 100 s^{-1} than between 100 and 200 s^{-1}, demonstrating that the BMF effectively replicates the physiological shear-thinning behavior of blood at moderate to high shear rates.

The sedimentation experiments indicated sedimentation effects at low shear rates of 1 s^{-1}. This can be attributed to density differences and transient start-up effects. However, compared to the quiescent sedimentation velocity, sedimentation tendency was less pronounced. At shear rates above 10 s^{-1} the viscosity remains constant, confirming no pronounced sedimentation effects under physiological shear conditions. This stability can be attributed, at least in part, to the high particle concentration in the BMF (40% (v/v)), which enhances

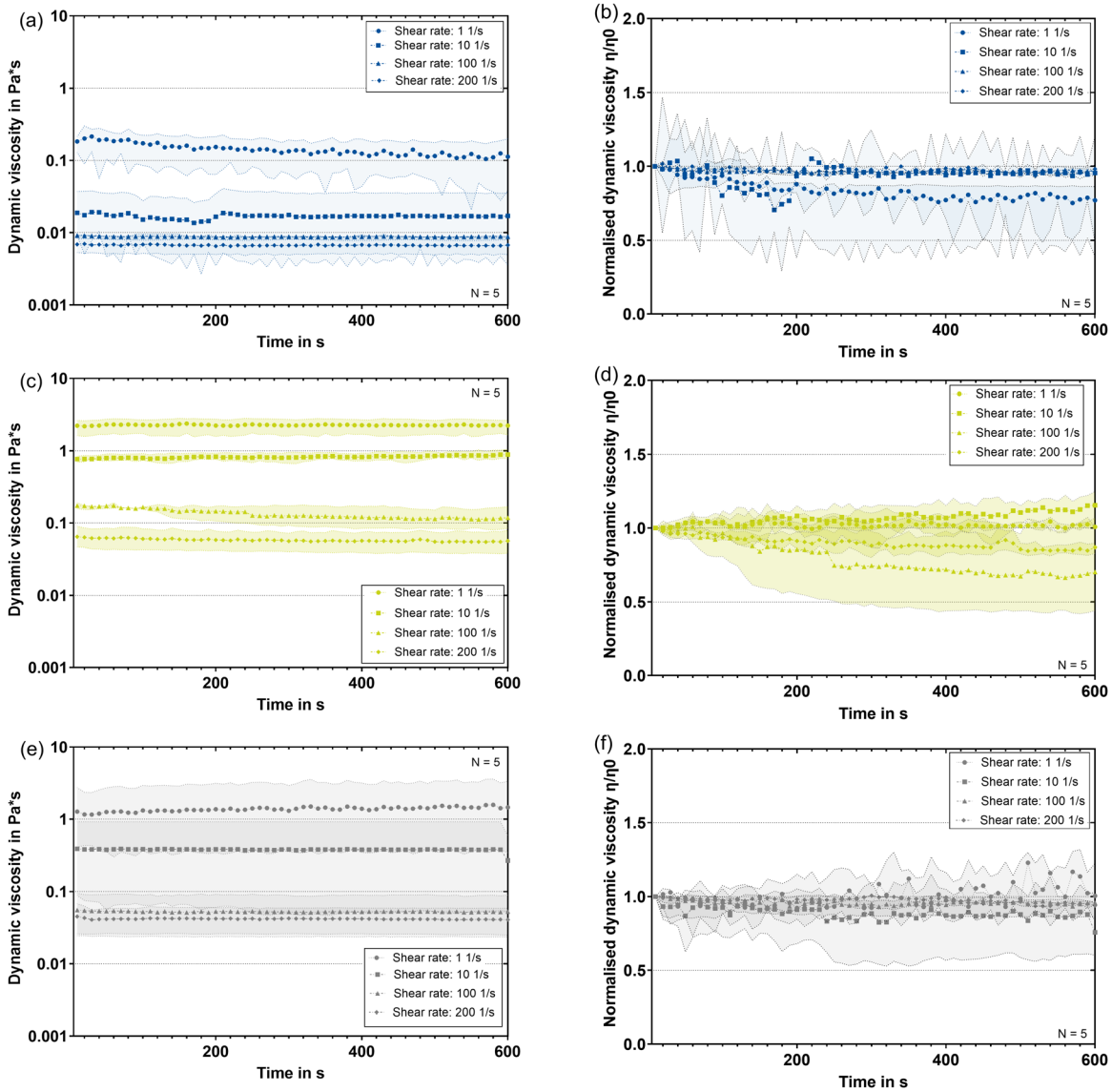

Fig. 5 (a) Particle sedimentation of microparticles dispersed in Dextran40/$CaCl_2$ solution (c) in glycerol 10% (v/v) solution and in (e) in glycerol 50% (v/v) solution. Measured over a 10-minute interval at four shear rates. Normalized viscosity over time for the microparticles dispersed in (b) Dextran40/$CaCl_2$, in (d) glycerol 10% (v/v) solution and in (f) glycerol 50% (v/v) solution. The normalized viscosity highlights viscosity changes over the 10-min measurement time. The dotted lines show the minimum and maximum values for every shear rate.

particle interactions, like particle repulsions as described by Fukada *et al.*[17] and hinders sedimentation.[43] These findings provide preliminary evidence that the Dextran 40/$CaCl_2$ BMF effectively mimics the shear-dependent viscosity and stability of whole blood across a range of physiological shear rates, thereby supporting its use in flow modeling studies.

At lower shear rates of 1 s^{-1} and 10 s^{-1}, the median viscosity value for the 10% (v/v) glycerol model was calculated to be higher than the mean viscosity value of the 50% (v/v) glycerol model. This is despite the fact that the glycerol 50% solution has a higher density (1.1092 g cm^{-3}) compared to the 10% solution (1.0205 g cm^{-3}). However, the viscosity values for the 50% glycerol model exhibit significant measurement variability, which reduces the reliability of these values. Higher glycerol concentrations in the artificial plasma phase appear to introduce more pronounced fluctuations in viscosity measurements. This effect is observed in both absolute and normalized shear-thinning values. Given the larger particle size, the establishment of a fully developed flow within the plate–plate geometry requires more time, leading to inconsistencies in viscosity measurements at low shear rates. Density comparisons further support these findings. The density difference between the microparticles and the 50% (v/v) glycerol solution is 8.85%, whereas the density difference between the microparticles and the 10% (v/v) glycerol solution is lower, at 6.53%. Despite the closer density match between the hydrogel particles and the 10% glycerol solution, sedimentation effects were observed in this model at shear rates of 100 and 200 s^{-1}, as indicated by a

decrease in normalized viscosity values over time. This suggests that, even with a relatively well-matched density, the large particle size contributes significantly to sedimentation. Consequently, the 10% glycerol model exhibits instability as a BMF due to pronounced sedimentation effects. In contrast, no significant sedimentation effects were observed in the 50% glycerol model, as evidenced by stable normalized shear-thinning values. The sedimentation tendency has decreased in comparison to quiescent conditions. The overall higher viscosity of the glycerol 50% (v/v) solution appears to stabilize the hydrogel particles within the artificial plasma phase, despite the greater density mismatch.

Ultimately, the large particle size resulted in inconsistencies in the viscosity profile, particularly in the lower-viscosity glycerol 10% (v/v) plasma phase. This instability limits the usability of both glycerol-based models as stable BMFs, as sedimentation effects compromise flow consistency in the 10% glycerol model, while high measurement variability due to pronounced start up effects reduces reliability in the 50% glycerol model.

However, shear thinning effects are evident for both BMFs as the shear rate increases, while the overall viscosity of both glycerol BMFs is considerably higher for all investigated discrete shear rates in comparison to the data presented by Nader *et al.*[42] Due to the particle size and shape of the artificial erythrocytes, particle interactions and deformations can occur that couldn't be detected with the experimental design of this study.

To the best of the authors knowledge, no studies have yet investigated the flow behavior of BMFs over extended measurement periods at constant shear rates. Such a characterization protocol could be critically important for ensuring that observed shear-thinning behavior is attributable to dynamic particle interactions rather than pronounced sedimentation effects.

Fukada *et al.*[17] reported a shift in the flow behavior of a polystyrene particle/$CaCl_2$ BMF from Newtonian to shear – thinning as the molecular weight of the particles increased. Investigating the sedimentation behavior of these systems could provide additional insights into the stability of such solutions, further elucidating the relationship between particle properties and their rheological behavior.

3.3.2 Dynamic shear behavior. Both glycerol-based artificial plasma phases exhibited Newtonian flow behavior (Fig. 6), where increasing water concentration resulted in decreased viscosity without altering the Newtonian characteristics. This

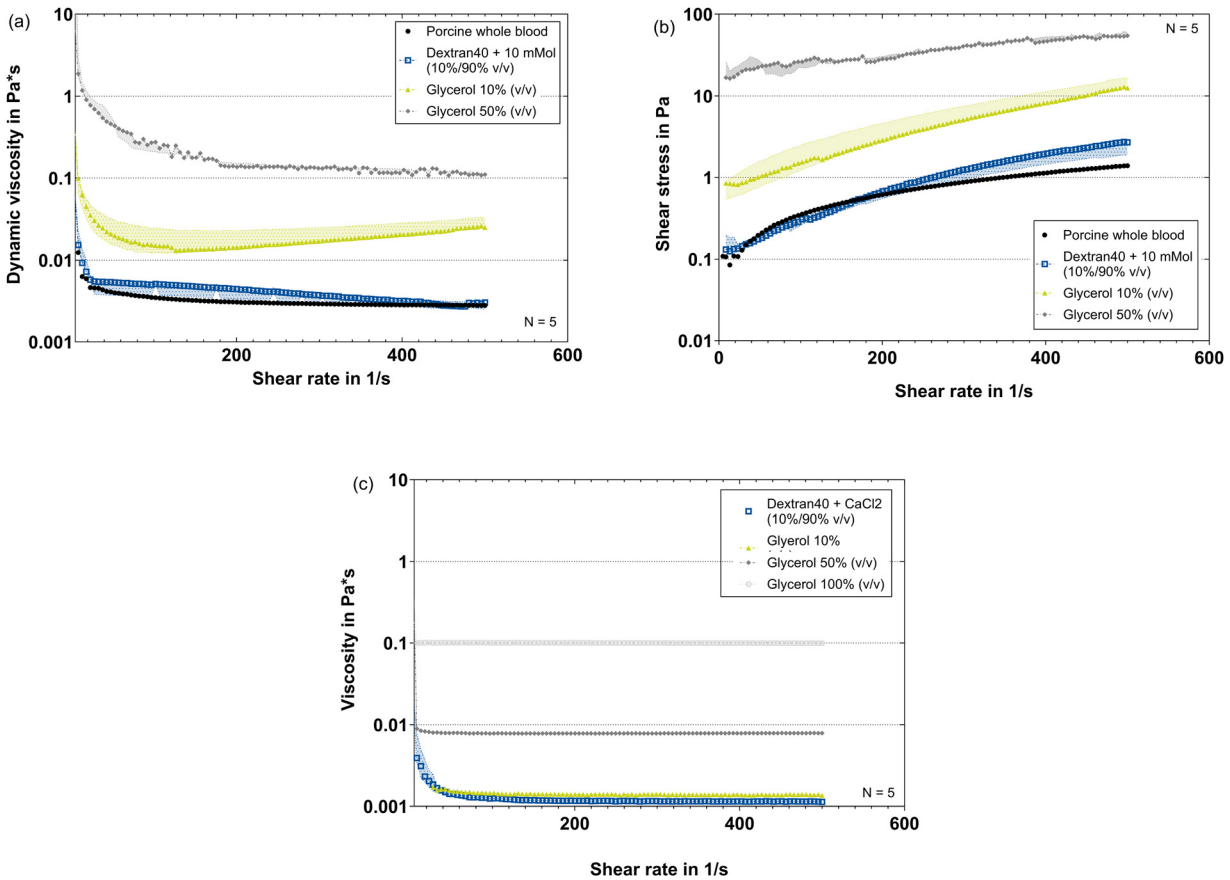

Fig. 6 (a) Shear behavior of the three blood mimicking fluids (BMF) compared to the porcine whole blood. (b) Shear stress behavior under shear flow. (c) Shear behavior of the artificial plasma phases. 100% (v/v) glycerol plot as negative control. Due to the lower torque limit of the rheometer, viscosity measurements for the 10% (v/v) glycerol solution could not be obtained at shear rates below 20 s^{-1}. The dotted lines show the minimum and maximum values for every shear rate.

is expected, as glycerol is a small organic molecule that forms a simple homogeneous solution rather than complex macromolecular structures capable of shear-induced alignment. Unlike polymer solutions, glycerol–water mixtures do not exhibit molecular entanglement or network formation, which are key mechanisms behind shear-thinning behavior.[44] Due to the lower torque limit of the rheometer, viscosity measurements for the 10% (v/v) glycerol solution could not be reliably obtained at shear rates below 20 s^{-1}.

In contrast, the Dextran40/$CaCl_2$ plasma model displayed slight shear-thinning behavior at lower shear rates (Fig. 6). This shear-thinning can be attributed to polymer–solvent interactions, where dextran molecules form hydrogen bonds with water, creating an interconnected network structure.[45] Additionally, as shear rate increases, dextran molecules align with the flow direction, which further enhances shear-thinning.[46] The viscosities of both the Dextran40/$CaCl_2$ solution and the 10% (v/v) glycerol solution are comparable to literature values for human blood plasma viscosity, which range from 1.2 to 1.7 mPa s at 37 °C,[42,47] making them suitable plasma mimics.

Upon adding artificial hydrogel erythrocytes to the plasma solutions, all three BMFs displayed shear-thinning behavior (Fig. 6). The overall viscosity values for the glycerol-based BMF models were higher than those of the porcine blood control, with viscosity increasing alongside glycerol concentration.

The 10% glycerol BMF, showed an increase in viscosity at higher shear rates ($\sim$200 s^{-1}). At these elevated shear rates, hydrodynamic forces can overcome the repulsive interactions between the negatively charged P(SA-Am) microparticles, allowing the particles to form clusters. This clustering leads to particle crowding, where particles align and form a more solid-like structure as stress increases.[48] Notably, this effect was absent in the 50% glycerol solution, indicating that the higher viscosity of the surrounding fluid maintains the repulsive forces between microparticles, thus preventing clustering even at high shear rates.

The shear stress against shear rate plots reveal yield stress fluid behavior in all three BMF models (Fig. 6). The yield stress (τ_0), or the stress required to initiate flow, for the Dextran40/$CaCl_2$ suspension was comparable to that of the porcine blood control. However, the yield stress values for both glycerol-based BMFs were significantly higher. For comparison, literature values for human blood yield stress range from 0.0018 to 0.031 Pa.[49,50] This suggests that while the Dextran40/$CaCl_2$ model approximates the yield stress of blood well, the glycerol-based models, especially at higher concentrations, deviate from physiological conditions due to their higher yield stress.

The experimental shear flow data was fitted against the Casson model to assess the flow characteristics of the three BMFs. Results are presented in Fig. 7. For the Dextran40/$CaCl_2$

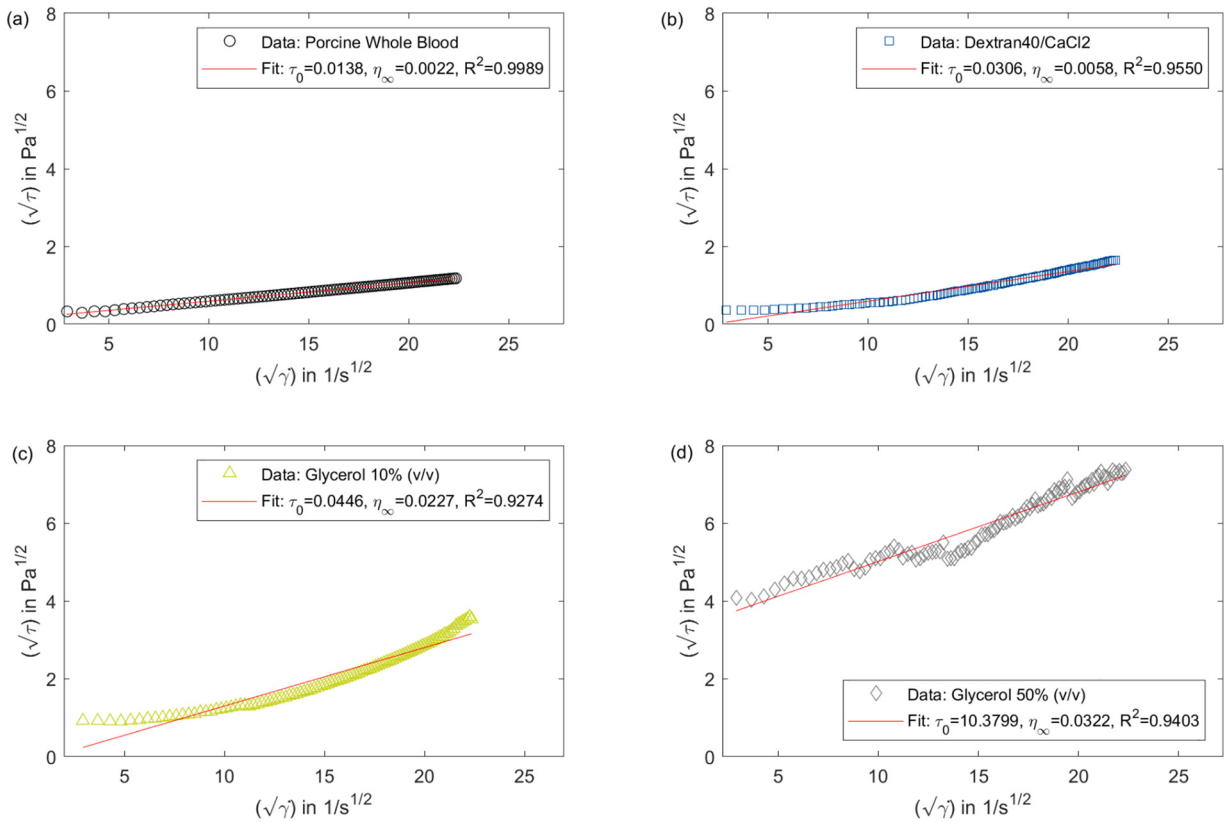

Fig. 7 Casson model fits (red line) for shear stress *vs.* shear rate for porcine whole blood and blood-mimicking fluids (BMFs). (a) Shows the porcine whole blood control, (b) the Dextran40/$CaCl_2$ model, (c) and (d) the glycerol models with 10% and 50% (v/v), respectively. The fitted yield stress and infinite viscosity values are displayed together with the R^2-value.

BMF, the yield stress (τ_0 = 0.0306 Pa) is slightly above the typical range for human blood but still within the bounds of literature values. The infinite shear viscosity (η_∞ = 0.0058 Pa s) is also slightly higher than typical values for human blood, which range from 3.5 to 5.5 mPa s.[42] The high R^2 value (0.9550) indicates a strong correlation, supporting the fit of the Casson model to the data.

In contrast, the 10% glycerol model shows higher yield stress (τ_0 = 0.0446 Pa) and infinite viscosity (η_∞ = 0.0227 Pa s) compared to both porcine blood and the Dextran40/$CaCl_2$ solution, indicating greater resistance to flow. While the R^2 value (0.9274) suggests a reasonable fit to the model, these physical parameters are notably different from those of blood, suggesting that the 10% glycerol BMF may be less suitable as a blood-mimicking fluid. The 50% glycerol model displays even greater divergence, with a very high yield stress (τ_0 = 10.3799 Pa) and infinite viscosity (η_∞ = 0.0322 Pa s). This substantial resistance to flow further deviates from human blood properties, despite the reasonable R^2 value (0.9403). The high values for both yield stress and viscosity indicate that the 50% glycerol model is unlikely to serve as an effective mimic for typical blood flow conditions.

Among the three BMFs, Dextran40/$CaCl_2$ shows the closest rheological properties to human blood, making it the most suitable candidate for simulating physiological conditions. The glycerol-based solutions, particularly at higher concentrations, show significant deviations from porcine blood properties, with increased infinite viscosity observed with higher glycerol concentrations.

Table 3 Carreau–Yasuada-model property results: comparison of the fit quality and specific parameters

Sample	η_0 (Pa s)	η_∞ (Pa s)	λ	n	a	R^2
Porcine whole blood	0.14841	0.0022572	8.5222	0.3	3	0.88192
Dextran40/$CaCl_2$	0.19357	0.002809	7.9343	0.3	2.8662	0.85187
Glycerol 10% (v/v)	0.72185	0.011721	4.2963	0.3	3	0.61031
Glycerol 50% (v/v)	1	0.001	0.59505	0.3	3	0.8363

In addition to the Casson model, the experimental data were also fitted using the Carreau–Yasuda model, as shown in Fig. 8. Key parameters and fit quality data are summarized in Table 3. The use of both models allows for a comprehensive analysis, as the Casson model is typically better suited for describing blood behavior at low shear rates, while the Carreau–Yasuda model provides a more accurate fit at higher shear rates.[23,51] This dual-model approach provides insights into the shear-dependent flow characteristics of BMFs across a range of conditions.

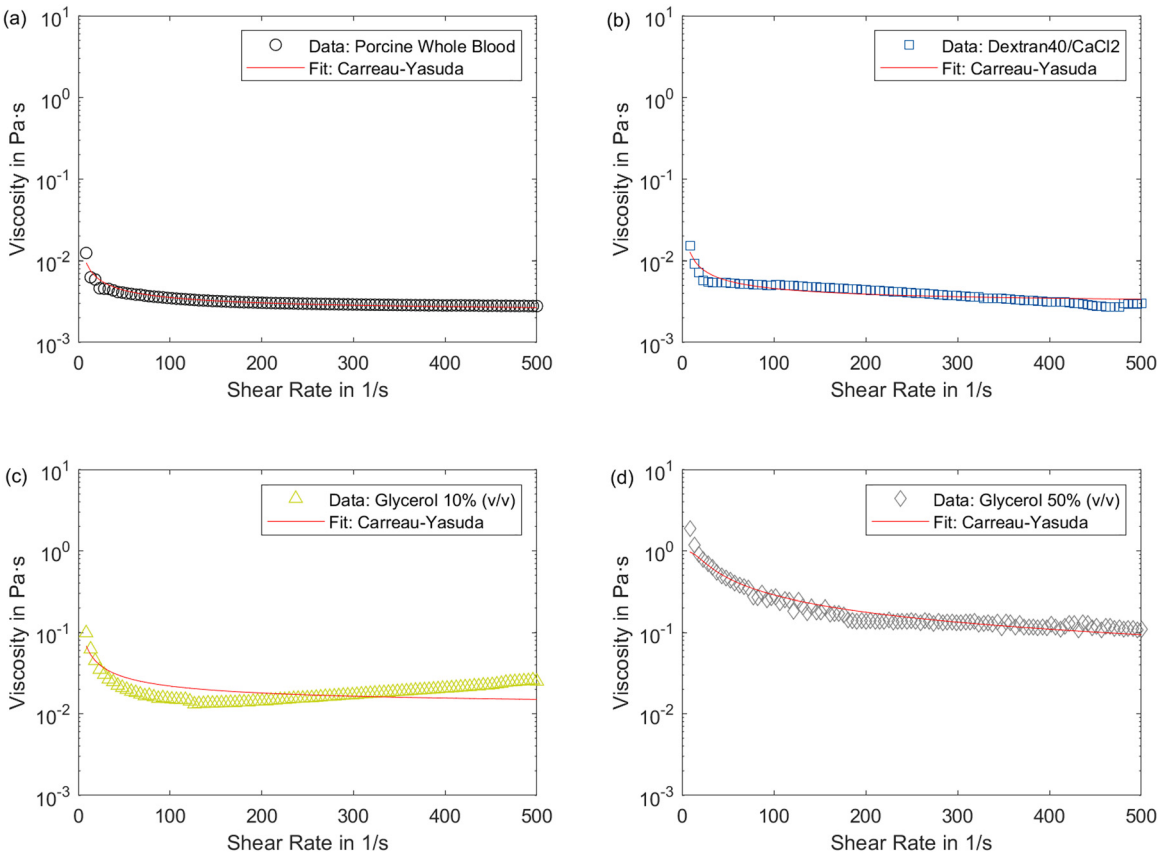

Fig. 8 Carrau–Yasuda model fits (red line) for viscosity *vs.* shear rate for blood-mimicking fluids (BMFs) and the positive control. (a) Shows the porcine whole blood control, (b) the Dextran40/$CaCl_2$ model, (c) and (d) the glycerol models with 10% and 50% (v/v), respectively. All curves are fitted against the same *y*-axis scaling for better comparison.

For the Dextran40/$CaCl_2$ BMF, the Carreau–Yasuda model calculated a zero shear viscosity of η_0 = 0.19357 Pa s. This value is slightly lower than the calculated value for porcine whole blood (η = 0.14841 Pa s) but still within the range of reported literature values for human blood zero shear viscosity, which is reported to be between 0.1–0.2 Pa s depending on the hematocrit level.[52] The Carreau–Yasuda model calculates a smaller value for the infinite shear viscosity compared to the Casson model. This results in a lower estimate for infinite viscosity for the Dextran40/$CaCl_2$ BMF. This calculated value is slightly below the reported literature values for the infinite viscosity of human blood but closely aligns with the results for the positive control. The power index from the Carreau–Yasuda model indicates shear-thinning behavior for the Dextran40/$CaCl_2$ BMF, which is consistent with the positive control. This is also in line with literature values for human whole blood, where the power index ranges between 0.3 and 0.4,[53] supporting the suitability of the Dextran40/$CaCl_2$ BMF. The R^2 value further indicate a strong fit to the rheological data of the Dextran40/$CaCl_2$ BMF.

In contrast, for the 10% (v/v) glycerol BMF, the Carreau–Yasuda model yielded significantly higher values for both zero shear viscosity and infinite viscosity compared to porcine blood and reported literature values. The model fit for this fluid showed lower infinite viscosity values than the Casson model, with a relatively low R^2 value (0.6103) suggesting a poor fit. These results indicate that the 10% glycerol BMF may not accurately replicate blood flow behavior, particularly at lower shear rates.

The fit for the 50% (v/v) glycerol BMF showed very high zero shear viscosity but a very low infinite viscosity, resulting in a very poor fit. This makes it unsuitable for mimicking normal blood conditions, despite a power index that indicates some similarity in shear-thinning behavior.

Both flow models demonstrate that the Dextran/$CaCl_2$ BMF is the only one of the three proposed blood-mimicking models that effectively mimics blood rheology across a broad range of shear rates. The results indicate that the presence of glycerol in the suspending medium (10% and 50% solutions) significantly impacts the rheological properties, especially for yield stress and zero shear viscosity. The high yield stress observed in the glycerol-based models, particularly in the 50% (v/v) solution, is partly due to the increased viscosity associated with higher glycerol concentrations, as shown in Fig. 6 and the high calculated values for the zero shear viscosity. Additionally, particles in the glycerol suspensions have swollen significantly, resulting in larger particle diameters (Fig. 4) and leading to shear induced clustering of particles at lower shear rates.[48] Further extensional rheology measurements on these plasma fluids could provide deeper insights into properties such as relaxation times, which influence the distinction between solid-like behavior below the yield stress and fluid-like behavior above the yield stress.[54]

The greatest differences among the BMFs emerged in their shear rheological behavior, particularly in yield stress, underscoring the significant influence of the plasma phase on fluid properties. The observed shear-thinning behavior of all BMFs upon the addition of artificial erythrocytes highlights the interplay between plasma composition, microparticle interactions, and flow dynamics, reflecting the key rheological feature of blood under shear flow. Beris *et al.*[49] identified fibrinogen as a key factor in rouleaux formation, which directly affects yield stress in blood. Similarly, as described by Fukada *et al.*,[17] Dextran 40 can facilitate interparticle bridging between beads in the BMF, potentially mimicking the role of fibrinogen. These results suggest that structural changes at the microscale, governed by interparticle interactions, translate into macroscopic rheological properties. Future studies should investigate the impact of Dextran 40 concentration on the yield stress behavior of the BMF to further refine its physiological relevance. Beyond fibrinogen, recent findings suggest that additional factors, such as mean corpuscular hemoglobin, may also play a role in blood rheology. Farrington *et al.*[55] demonstrated through neural network-based analysis that hemoglobin concentration within RBCs could influence flow properties. Incorporating hemoglobin into artificial erythrocytes could further enhance the physiological accuracy of BMFs, providing a more comprehensive model while also facilitating data generation for machine-learning approaches in blood rheology modeling.

Extensional rheometry could provide additional insights into the rheological profiles of BMF models, particularly for parameters like relaxation time, which are essential for accurately mimicking blood plasma.[9,56] So far, only a study by Carneiro *et al.*[9] investigated their BMF (Table 1) in extensional flow. They reported a relaxation time of approximately 310 μs for their BMF model,[9] whereas literature values for human whole blood indicate a relaxation time of 114 μs.[56] This represents a substantial difference compared to the relaxation times fitted in the Carreau–Yasuda model, which ranged between 0.595 and 7.934 s for the three BMFs. In the Carreau–Yasuda model, relaxation time characterizes the transition from Newtonian to power-law behavior in shear flow. However, in extensional rheology, the measured relaxation time is more directly related to the molecular relaxation of stretched polymer chains. Given this distinction, additional extensional

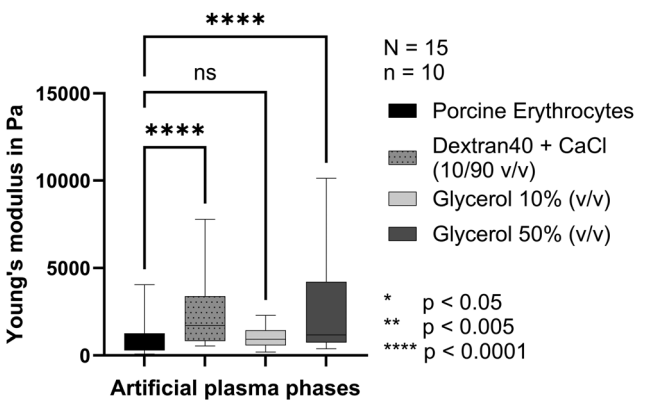

Fig. 9 Young's modulus of the artifical erythrocytes after swelling in the respective plasma phases. The Young's modulus was measured after the particles sedimented to the Petri dish ground.

flow measurements would provide further insight into the viscoelastic behavior of our BMF and enhance its characterization.

Our study achieves a rheological match to blood despite the larger particle size by matching parameters such as particle volume fraction and plasma composition. Wu *et al.*[35] demonstrates how non-Newtonian flow properties are critical in determining hemodynamic relevance. Our study prioritizes matching blood's rheological behavior, including shear-thinning effects and yield stress, which are key to mimicking real blood behavior *in vitro*.

3.4 Mechanical characterization

In addition to rheological characterization, this study sought to match the elastic properties of the artificial erythrocytes to those of blood as closely as possible. Although there are no studies directly measuring the Young's modulus of porcine erythrocytes, they are commonly used as substitutes for human erythrocytes due to their similar rheological behavior. Therefore, we compared our results with published Young's modulus values for human erythrocytes. Sergunova *et al.*[57] reported an average Young's modulus of 2.597 ± 1.221 kPa for healthy human erythrocytes, while Barns *et al.*[58] observed a higher average of 7.57 ± 3.25 kPa for glutaraldehyde – fixed erythrocytes, which likely reflects the stiffening effect of fixation. In general, the literature shows a broad range of values for the Young's modulus of human erythrocytes, from 0.1–0.2 kPa[59] to as high as 202.40 kPa,[60] highlighting significant variability. The average Young's modulus of 0.91 kPa measured for porcine erythrocytes in this study falls within the lower range of reported values.

BMFs dispersed in the 10% (v/v) glycerol/water solution demonstrated the closest match to porcine erythrocytes, with an average Young's modulus of 0.991 kPa. Statistical analysis revealed no significant difference between this BMF and the porcine control, suggesting that the 10% glycerol solution effectively replicates the mechanical properties of native erythrocytes (Fig. 9). Furthermore, force–distance curves indicated that repeated mechanical loading did not induce plastic deformation in the artificial erythrocytes (ESI,† S1 Elasticity curves), confirming their elastic behavior.

The artificial erythrocytes dispersed in the Dextran40/$CaCl_2$ solution exhibited a higher average Young's modulus of 2.233 kPa (Fig. 9). This increase in stiffness can be attributed to the ionic cross-linking effects of $CaCl_2$, as described by Trivedi and Chourasia,[33] who found that hydrogels in $CaCl_2$ become harder and more rubbery due to additional ionic cross-linking at the particle surface. Although the Young's modulus for this BMF was significantly different from the porcine control, it still falls within the broad range reported for human erythrocytes. The artificial erythrocytes in this solution also demonstrated elastic deformation under repeated mechanical loading (ESI,† S3 Elasticity curves). The artificial erythrocytes dispersed in the 50% (v/v) glycerol solution had an average Young's modulus of 2.66 kPa, indicating significantly greater stiffness compared to the porcine control (Fig. 9). However, these measurements displayed considerable variability, which should be considered when interpreting the results. The increased glycerol concentration likely contributes to the enhanced stiffness. As Xu *et al.*[61] observed that higher glycerol levels increase mechanical strength by disrupting hydrogen bonds within polymer chains, thereby enhancing polymer chain flexibility and improving stress distribution under load. In the P(SA-Am) hydrogel used for the artificial erythrocytes, the amide groups (–$CONH_2$) in acrylamide can act as hydrogen bond donors, while the carbonyl oxygen (C═O) serves as a hydrogen bond acceptor, contributing to the material's mechanical response.

The Young's modulus, which measures membrane elasticity and thus RBC deformability, is an important parameter in blood flow simulation. Several hereditary and metabolic disorders such as stomatocytosis and diabetes are directly linked to the impairment of particle deformability.[62] Mechanical properties of RBCs also correlates with the likelihood of strain-induced cell damage, such as hemolysis.[63] A study from Kanais *et al.*[64] suggested that RBCs with higher Young's modulus are more prone to reach critical strain thresholds where hemolysis occurs. Consequently, accurately replicating the mechanical properties of RBCs in BMFs is essential for realistic simulation of blood behavior and for predicting mechanical stresses in applications such as medical device testing or microvascular flow studies.

The artificial erythrocytes dispersed in the Dextran40/$CaCl_2$ and the glycerol 10% (v/v) solutions demonstrate a close approximation to the elastic response of human and porcine erythrocytes, exhibiting a greater degree of elasticity than the BMF's from Doshi *et al.*[13] and Chen *et al.*[8] (Table 1).

4 Conclusions

This study evaluated three blood-mimicking fluids (BMFs) based on their particle size, shape, rheological, and mechanical properties to identify a model that replicates blood's characteristics as comprehensively as possible. Among the fluids tested, the BMF consisting of P(SA-Am) hydrogel beads as artificial erythrocytes dispersed in a Dextran40/$CaCl_2$ solution proved to be the most suitable option. Its rheological and mechanical properties align closely with those of human blood. Despite the current limitations in particle size, the proposed BMF demonstrates a versatile range of well-matched parameters, including shape, rheological, and mechanical properties, in comparison to previously established BMFs discussed in Table 1. While the rheological and mechanical properties of the proposed BMF suggest that axial migration and CFL formation should occur under flow conditions, these effects were not explicitly visualized in this study. The shear-thinning behavior observed in the Dextran40/$CaCl_2$ BMF closely resembles the shear-dependent migration dynamics of RBCs, which drive CFL formation in microvascular systems. Prior work on particulate blood analogs has demonstrated that rheologically matched suspensions can successfully replicate CFL formation and RBC-like migration in

microfluidic flow studies.[10] Future studies will focus on direct imaging of CFL formation and RBC-like migration using microfluidic channels and high-speed microscopy to further validate the multiphase behavior of the proposed BMF. By systematically evaluating the relationship between plasma composition, microparticle elasticity, and shear response, this study advances the fundamental understanding of BMF design beyond simple viscosity matching. The ability to tune viscoelastic properties by modifying microstructure and interparticle forces provides a framework for designing BMFs that can better replicate blood dynamics across diverse experimental and clinical applications.

This study advances the development of BMFs by introducing a model that offers a wider replication of blood properties, making it a valuable tool for *in vitro* – blood flow studies. Future work will also focus on validating the BMF in controlled flow environments, ensuring its compatibility with established experimental techniques, such as PIV and other optical flow diagnostics. Next steps will evaluate the BMF in physiologically relevant conditions, including flow loop experiments and medical device testing. These studies will examine its behavior in artificial heart valves, stents, and other blood-contacting devices, with a particular focus on shear-dependent rheology, stability, and traceability within complex flow fields. The present study work lays the foundation for the use of the BMF in biomedical research, fluid dynamics studies, and medical device development.

Author contributions

GH and BG conceived this research; GH conducted the experiments; KN conducted the AFM measurements; GH performed initial data analysis, GH wrote the manuscript; KN, MM, PB and BG edited and reviewed the manuscript.

Data availability

Data supporting this article have been included as part of the ESI.†

Conflicts of interest

There are no conflicts of interest to declare.

Acknowledgements

The authors would like to thank the ''Caroline Herschel Foundation'' for funding this research. This work is partly funded by the Federal Ministry of Education and Research within the Forschungscampus STIMULATE (grant no. 13GW0473A). We would like to thank NETZSCH-Gerätebau GmbH for providing the rheometer and for their support with the rheological characterization (especially Gérald Chabanis) within the NBE Lab IMP cooperation. Additionally, the author would like to thank Christina Winkler for her support and Finja Stadtler and Vanessa Brandt for their support in conducting the microparticle fabrication.

Notes and references

1 K. Sriram, M. Intaglietta and D. M. Tartakovsky, *Microcirculation*, 2014, **21**, 628–639.
2 S. Lynch, N. Nama and C. A. Figueroa, *Sci. Rep.*, 2022, **12**, 20568.
3 S. S. Shibeshi and W. E. Collins, *Appl. Rheol.*, 2005, **15**, 398–405.
4 H. E. Salman and H. C. Yalcin, *Cardiovasc. Dev. Dis.*, 2021, **8**, 1–27.
5 C. A. Luisi, T. L. Witter, O. Nikoubashman, M. Wiesmann, U. Steinseifer and M. Neidlin, *Nat. Sci. Rep.*, 2024, 1–13.
6 P. Berg, S. Saalfeld, S. Voß, O. Beuing and G. Janiga, *Neurosurg. Focus*, 2019, **47**, E15.
7 S. H. Sadek, M. Rubio, R. Lima and E. J. Vega, *Materials*, 2021, **14**, 2451.
8 Q. Chen, N. Singh, K. Schirrmann, Q. Zhou, I. L. Chernyavsky and A. Juel, *Soft Matter*, 2023, **19**, 5249–5261.
9 J. Carneiro, R. Lima, J. B. L. M. Campos and J. M. Miranda, *Soft Matter*, 2021, **17**, 3963–3974.
10 V. Froese, G. Gabel, J. Parnell, A. Prause, M. Lommel and U. Kertzscher, *Exp. Fluids*, 2022, **63**, 188.
11 M. Schöps, J. Clauser, M. Menne, F. Faßbänder, T. Schmitz-Rhode, U. Steinseifer and A. Arens, *Biotechnol. J.*, 2020, **15**, 1900239.
12 S. V. Jansen, I. Müller, M. Nachtsheim, T. Schmitz-Rode and U. Steinseifer, *Artif. Organs*, 2016, **40**, 207–212.
13 N. Doshi, A. S. Zahr, S. Bhaskar, J. Lahann and S. Mitragotri, *Proc. Natl. Acad. Sci. U. S. A.*, 2009, **106**, 21495–21499.
14 Y. F. Jia, J. H. Jiang, X. D. Ma, Y. Li, H. M. Huang, K. B. Cai, S. X. Cai and Y. P. Wu, *Chin. Sci. Bull.*, 2008, **53**, 3928–3936.
15 K. V. Ramnarine, D. K. Nassiri, P. R. Hoskins and J. Lubbers, *Ultrasound Med. Biol.*, 1998, **24**, 451–459.
16 F. Knüppel, I. Thomas, F.-H. Wurm and B. Torner, *Fluids*, 2023, 1–14.
17 E. Fukada, G. V. Seaman, D. Liepsch, M. Lee and L. Friis-Baastad, *Biorheology*, 1989, **26**, 401–413.
18 G. Hentschel, M. Weiß, S. Hoffmann, W. Nahm and B. Glasmacher, *Curr. Dir. Biomed. Eng.*, 2023, **9**, 579–582.
19 M. B. Gallagher, K. I. Aycock, B. A. Craven and K. B. Manning, *Cardiovasc. Eng. Technol.*, 2018, **9**, 641–653.
20 M. Y. Yousif, D. W. Holdsworth and T. L. Poepping, *Exp. Fluids*, 2011, **50**, 769–774.
21 R. Lima, S. Wada, M. Takeda, K. I. Tsubota and T. Yamaguchi, *J. Biomech.*, 2007, **40**, 2752–2757.
22 K. Namdee, M. Carrasco-Teja, M. B. Fish, P. Charoenphol and O. Eniola-Adefeso, *Sci. Rep.*, 2015, **5**, 1–14.
23 J. Boyd, J. M. Buick and S. Green, *Phys. Fluids*, 2007, **19**, 093103.
24 J. Venkatesan, D. S. Sankar, K. Hemalatha and Y. Yatim, *J. Appl. Math.*, 2013, **2013**, 1–11.

25 H. Liu, L. Lan, J. Abrigo, H. L. Ip, Y. Soo, D. Zheng, K. S. Wong, D. Wang, T. W. Leung and X. Leng, *Front. Physiol.*, 2021, **12**, 718540.
26 B. Stemper, D. Board, N. Yoganandan and C. Wolfla, *J. Craniovertebr. Junction Spine*, 2010, **1**, 18–22.
27 M. Zagnoni, J. Anderson and J. M. Cooper, *Langmuir*, 2010, **26**, 9416–9422.
28 D. Dendukuri, K. Tsoi, T. A. Hatton and P. S. Doyle, *Langmuir*, 2005, **21**, 2113–2116.
29 C. Winkler, G. Hentschel, M. Müller, B. Glasmacher, P. Berg, K. Zähringer and F. Rummel, *iCCC2024 – iCampμs Cottbus Conference 2024*, 2024, vol. 1, pp. 108–111.
30 C. Uzoigwe, *Med. Hypotheses*, 2006, **67**, 1159–1163.
31 M. Diez-Silva, M. Dao, J. Han, C.-T. Lim and S. Suresh, *MRS Bull.*, 2010, **35**, 382–388.
32 R. Mahon, Y. Balogun, G. Oluyemi and J. Njuguna, *SN Appl. Sci.*, 2019, **2**, 1–15.
33 J. Trivedi and A. Chourasia, *Gels*, 2023, **9**, 1–17.
34 K. Bialik-Was, K. Pluta, D. Malina, M. Barczewski, K. Malarz and A. Mrozek-Wilczkiewicz, *Int. J. Mol. Sci.*, 2021, **22**, 1–18.
35 X. Wu, S. Gürzing, C. Schinkel, M. Toussaint, R. Perinajovaá, P. V. Ooij and S. Kenjereš, *Cardiovasc. Eng. Technol.*, 2022, **13**, 428–442.
36 L. Goubergrits, S. Weber, C. Petz, H.-C. Hege, A. Spuler, A. Berthe and U. Kertzscher, *J. Visualization*, 2009, **12**, 241–250.
37 O. Kašpar, A. H. Koyuncu, A. Hubatová-Vacková, M. Balouch and V. Tokárová, *RSC Adv.*, 2020, **10**, 15179–15189.
38 S. Tanriverdi, J. Cruz, S. Habibi, K. Amini, M. Costa, F. Lundell, G. Mårtensson, L. Brandt, O. Tammisola and A. Russom, *Microsyst. Nanoeng.*, 2024, **10**, 87.
39 F. Momen-Heravi, L. Balaj, S. Alian, A. J. Trachtenberg, F. H. Hochberg, J. Skog and W. P. Kuo, *Front. Physiol.*, 2012, **3**, 1–6.
40 T. Shajahan and W.-P. Breugem, *Flow, Turbul. Combust.*, 2020, **105**, 537–554.
41 S. Oka, *Biorheology*, 1985, **22**, 315–321.
42 E. Nader, S. Skinner, M. Romana, R. Fort, N. Lemonne, N. Guillot, A. Gauthier, S. Antoine-Jonville, C. Renoux, M.-D. Hardy-Dessources, E. Stauffer, P. Joly, Y. Bertrand and P. Connes, *Front. Physiol.*, 2019, **10**, 1329.
43 J.-C. Tsai, M.-R. Chou, P.-C. Huang, H.-T. Fei and J.-R. Huang, *Soft Matter*, 2020, **16**, 7535–7543.
44 M. Pagliaro and M. Rossi, *Glycerol: Properties and Production*, The Royal Society of Chemistry, 2008, pp. 1–17.
45 A. Farahnaky, Z. Allahdad, M. Aminlari, M. Majzoobi, H. Askari and R. Ramezani, *Int. J. Food Eng.*, 2012, **8**, 1–12.
46 V. Tirtaatmadja, D. E. Dunstan and D. V. Boger, *J. Non-Newtonian Fluid Mech.*, 2001, **97**, 295–301.
47 G. Késmárky, P. Kenyeres, M. Rábai and K. Tóth, *Clin. Hemorheol. Microcirc.*, 2008, **39**, 243–246.
48 V. Gopalakrishnan and C. F. Zukoski, *J. Rheol.*, 2004, **48**, 1321–1344.
49 A. N. Beris, J. S. Horner, S. Jariwala, M. J. Armstrong and N. J. Wagner, *Soft Matter*, 2021, **17**, 10591–10613.
50 B.-K. Lee, S. Xue, J. Nam, H. Lim and S. Shin, *Korea-Aust. Rheol. J.*, 2011, **23**, 1–6.
51 A. Fuchs, N. Berg, L. Fuchs and L. P. Wittberg, *Bioengineering*, 2023, **10**, 1–20.
52 E. W. Merrill, E. R. Gilliland, G. Cokelet, H. Shin, A. Britten and R. E. W Jr., *Biophys. J.*, 1963, **3**, 199–213.
53 S. Chien, *Red Blood Cells*, 1975, **2**, 1031–1133.
54 G. Pagani, M. Hofmann, L. E. Govaert, T. A. Tervoort and J. Vermant, *J. Rheol.*, 2024, **68**, 155–170.
55 S. Farrington, S. Jariwala, M. Armstrong, E. Nigro, N. J. Wagner and A. N. Beris, *Rheol. Acta*, 2023, **62**, 491–506.
56 P. C. Sousa, R. Vaz, A. Cerejo, M. S. N. Oliveira, M. A. Alves and F. T. Pinho, *J. Rheol.*, 2018, **62**, 447–456.
57 V. Sergunova, S. Leesment, A. Kozlov, V. Inozemtsev, P. Platitsina, S. L. A. Onufrievich, V. Polyakov and E. Sherstyukova, *Sensors*, 2022, **22**, 1–13.
58 S. Barns, M. A. Balanant, E. Sauret, R. Flower, S. Saha and Y. Gu, *Biomed. Eng. Online*, 2017, **14**, 1–21.
59 L. Mi, L. LianQing, X. Ning, W. YueChao, D. ZaiLi, X. XiuBin and Z. WeiJing, *Sci. China: Life Sci.*, 2012, **55**, 968–973.
60 C. C. Lien, M. C. Wu and C. Ay, *Adv. Dev. Ind. Appl. Mech.*, 2014, **627**, 197–201.
61 B. Xu, Y. Liu, L. Wang, X. Ge, M. Fu, P. Wang and Q. Wang, *Polymers*, 2018, **10**, 1–12.
62 G. Tomaiuolo, *Biomicrofluidics*, 2014, **8**, 051501.
63 Y. Chen and M. Sharp, *Artif. Organs*, 2011, **35**, 145–156.
64 T. Kanais, M. Lanteri, G. Page, Y. Guo, S. Endres, M. Stone, S. Keating, A. Mast, R. Cable, D. Triulzi, J. Kiss, E. Murphy, S. K. M. Bush and M. Gladwin, *Blood Adv.*, 2017, **1**, 1132–1141.

